Calculation of the Dynamic Loads acting upon a Rope Grip as it passes around the Bull Wheel on a Fixed Grip Quad Chair Lift

By

Peter Luger[1]

The Task

In the case of fixed grip chair lifts, the carriers pass around the bull wheels at full rope speed. The introduction of loading carpets made it possible to further increase rope speeds with a view to shortening trip times.

When passengers attempt to leave the lift at bull wheel exits, the relatively high rope speed leads to a risk of the passenger failing to vacate the chair in time and thus travelling around the bull wheel. If this happens, the centripetal acceleration in particular causes excessive wear on the grip, hanger arm and carrier.

The aim of this paper was to develop a method, and subsequently a computer program, which would make it possible to calculate the dynamic loads on the rope grip and hanger arm when the carriers travel around the bull wheel.

[1] Key Account Manager
ELB-Form GmbH
Riederstrasse 12
A-6773 Vandans / Austria

Tel.: +43 5556 77881-720
Fax: +43 5556 77881-701
e-mail: pluger@elb-form.at

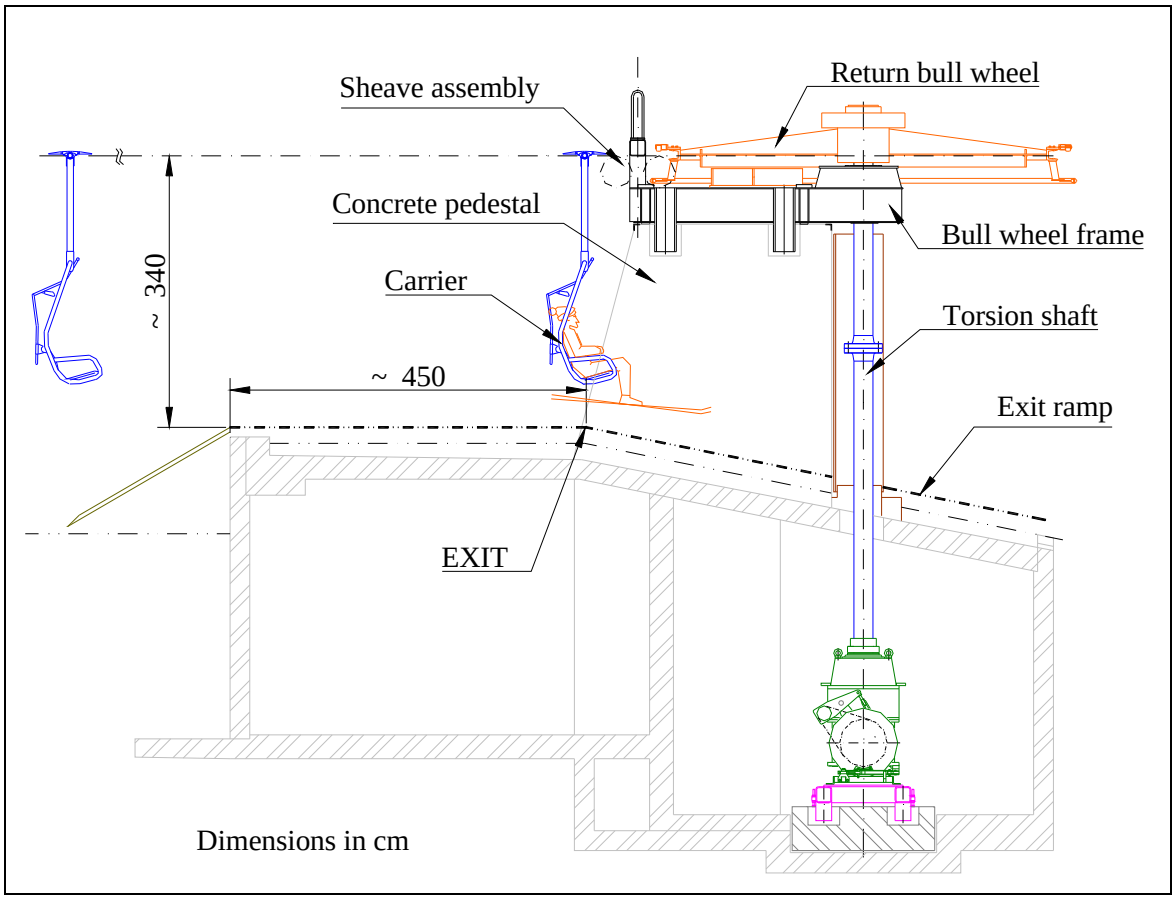

Fig. 1: Configuration of a bull wheel exit

The simulation program developed was verified by recalculating an existing installation, the 4-CLF quad chair lift Saloberkopf/Schröcken/Vorarlberg supplied by the Austrian manufacturer Doppelmayr of Wolfurt.

What happens when carriers pass around the bull wheel

Under normal conditions, the carriers travel through the station at a specific rope speed, which varies from 1.4 to 2.8 m/s, depending on the lift type. Once the skiers have vacated the chair, it leads into the bull wheel in a virtually perpendicular position with very little swing motion, then passes around it. The sudden deflection of the chair (angular acceleration $\dot{\Omega}$ theoretically ∞) and its entry into and pressure against the liner

as it passes around the bull wheel subjects it to a largely radial swing and produces torsional vibration about its vertical axis (see Fig. 2).

The radial swing of the chair is restricted by two design measures. The upper hold-down ring prevents an excessive outward swing while the lower guide ring ensures that the chair cannot swing too far under the bull wheel.

The bull wheel liner provides an elastic support for the rope. The position of the rope in the liner is guided by the incoming sheave assembly in such a way that the empty chair contacts neither the hold-down ring nor the guide ring when travelling at nominal speed.

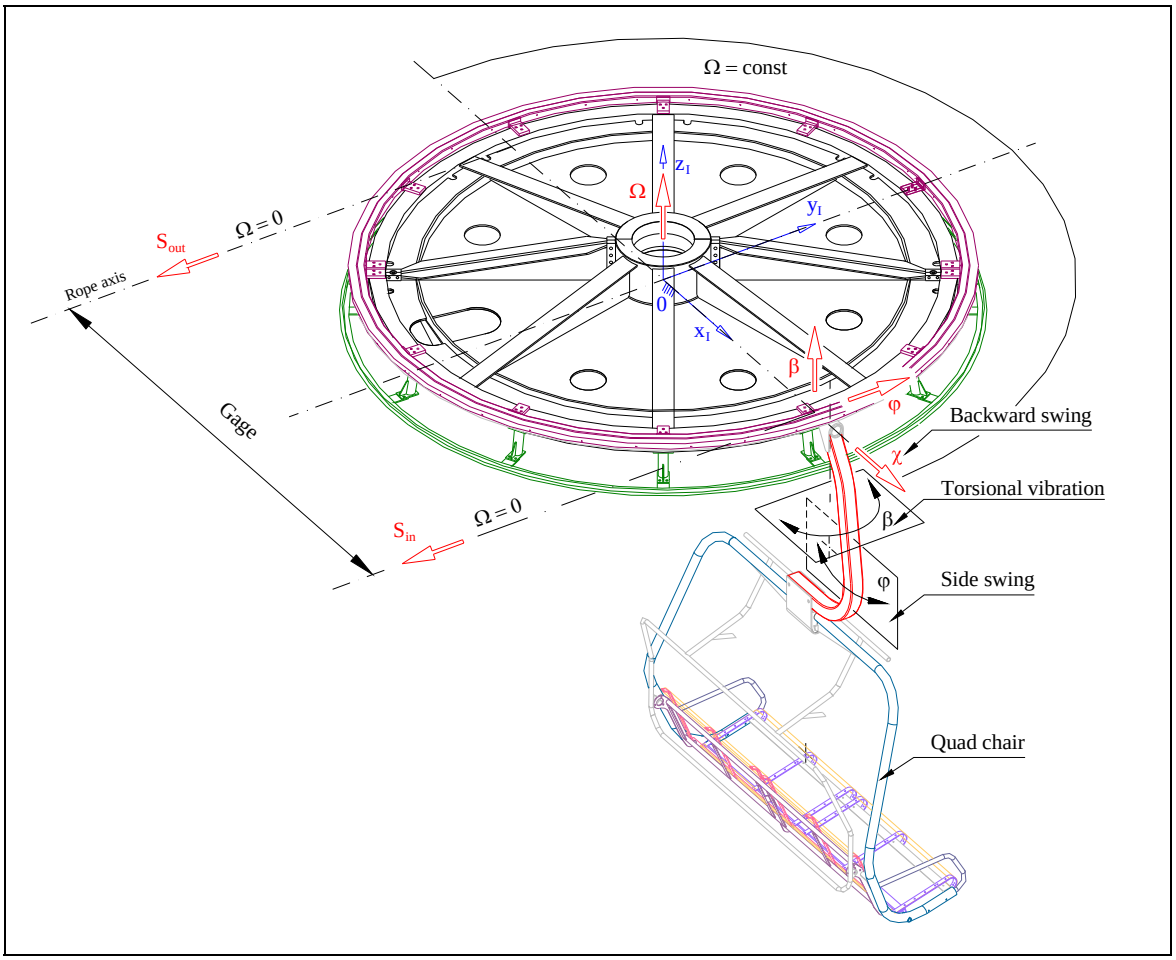

Fig. 2: What happens when a carrier passes around the bull wheel

When the grip enters the bull wheel, i.e. contacts the liner, the shape of the grip causes the rope center to move outwards and to lift off in this area. The liner offers resistance to the swing motion and to the torsional vibrations about the vertical axis of the chair.

When the chair exits the bull wheel it is subjected to a dynamic load change and the torsional vibration is again activated. This vibration then decreases relatively quickly and the chair proceeds on its journey downhill.

Simulation Model

In order to calculate the dynamic loads on the rope grip, it is necessary to apply the equations of motion for all moving parts. Initially, it is possible to assume that these parts, in particular the grip, hanger and chair, behave like rigid bodies.

The bull wheel is assumed to be rigid. Thus it will only be necessary to formulate equations of motion for the bodies of the grip, hanger and chair.

From an engineering perspective, parts which display an elastic or spring-type behavior can be replaced by zero-mass springs. The liner, guide ring and hold-down ring are replaced by springs which demonstrate a nonlinear behavior resulting from the rubber liner material and the partly discrete operating cycle. In order to calculate the stiffness of these springs, the finite element method is used in part.

The multiple-body system had to possess at least 3 degrees of freedom (DOFs) if it was to be able to simulate all the effects described above. The following position coordinates, corresponding to the three rotational DOFs are used for the simulation program (see Fig. 3):

- φ … side swing,
- β … rotational DOF about the vertical axis of the chair,
- χ … longitudinal swing.

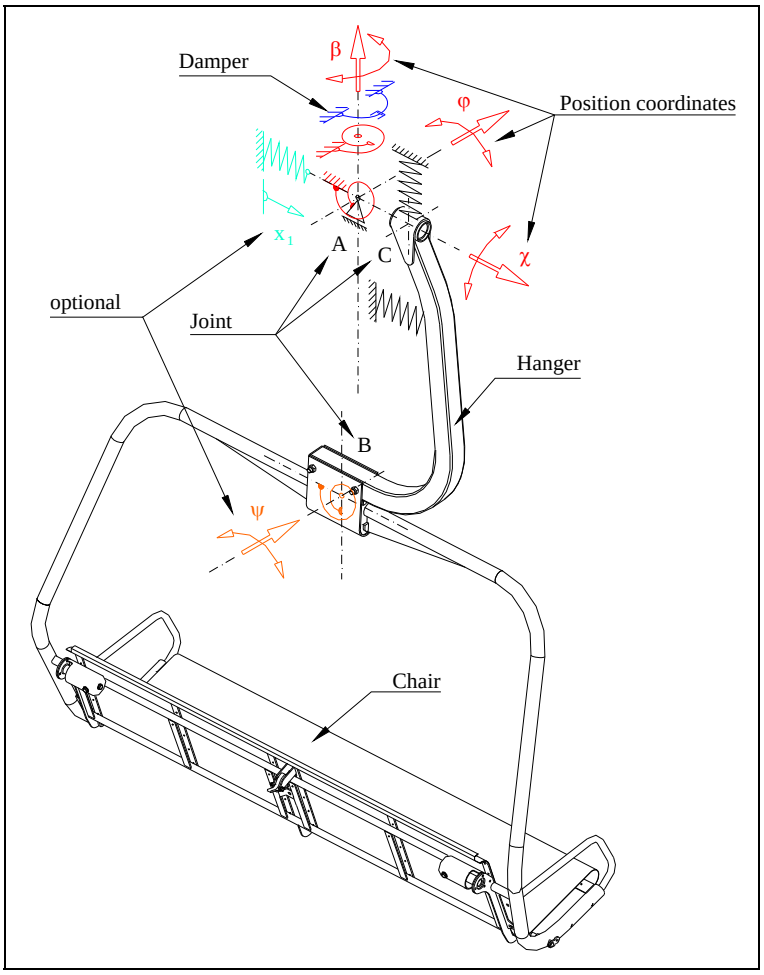

Fig. 3: Sketch of simulation model (rigid bodies, zero-mass springs)

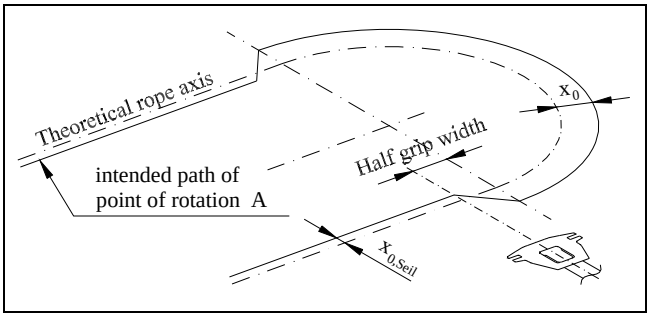

Fig. 4: Sketch of intended movement of point of rotation A

As the translational DOF with the position coordinate x_1 has not been included, the radial displacement of the point of rotation *A* must be assigned as the intended movement (see Fig. 4). This makes it possible to approximately reflect some of the

effects on entry into the bull wheel, such as the almost jolt-like outward displacement of the grip.

Moment Characteristic of the Liner

A rotation of the grip about the rope axis is opposed by a righting moment from the liner. There are several difficulties inherent in the calculation of this moment in relation to the angle φ. The main problem lies in the fact that, irrespective of the model dimension (2-D or 3-D), characteristics would have to be calculated in the form of complex contact problems depending on the radial pressure resulting from rope tension and the angle φ. This moment characteristic was therefore measured (see Fig. 5 for test configuration).

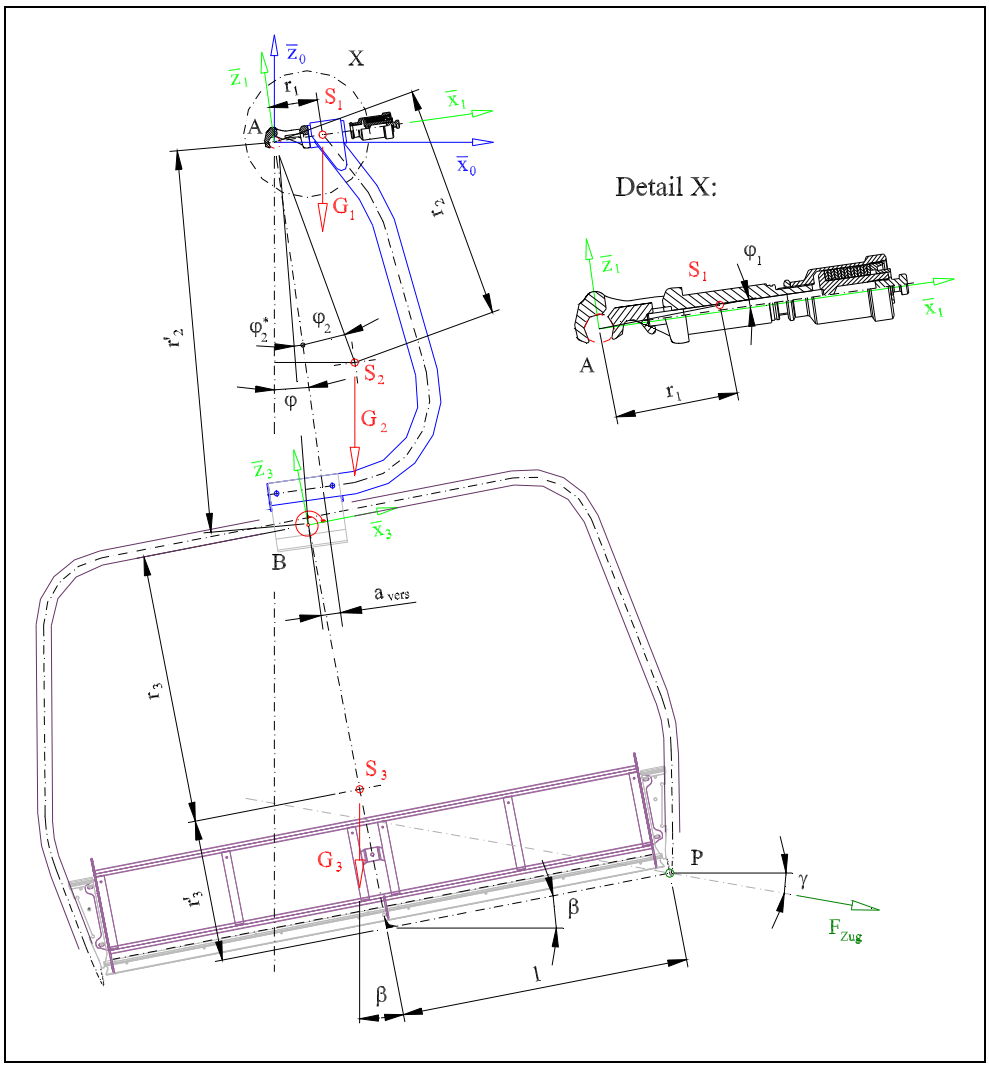

Fig. 5: Sketch of carrier pull test

With known geometry and body weights, the required characteristic curve can be calculated by assuming a static state of equilibrium at suspension point A.

Equilibrium of moments

$$\left(\sum M\right)_A = f\left(\varphi\right) \qquad (1)$$

gives

$$\begin{aligned} M_A(\varphi) = M_{y,A} = {} & G_1 r_1 \cos\left(\varphi + \varphi_1\right) + G_2 r_2 \sin\left(\varphi + \varphi_2\right) + G_3 \left[r_2' \sin\left(\varphi - \varphi_2^*\right) + r_3 \sin\beta\right] + \\ & + F_{Zug} \sin\gamma \left[r_2' \sin\left(\varphi - \varphi_2^*\right) + \left(r_3 + r_3'\right)\sin\beta + l\cos\beta\right] - \\ & - F_{Zug} \cos\gamma \left[r_2' \cos\left(\varphi - \varphi_2^*\right) + \left(r_3 + r_3'\right)\cos\beta - l\sin\beta\right]. \end{aligned} \qquad (2)$$

An overview of the measuring points and the individual moment curves is shown in Fig. 6.

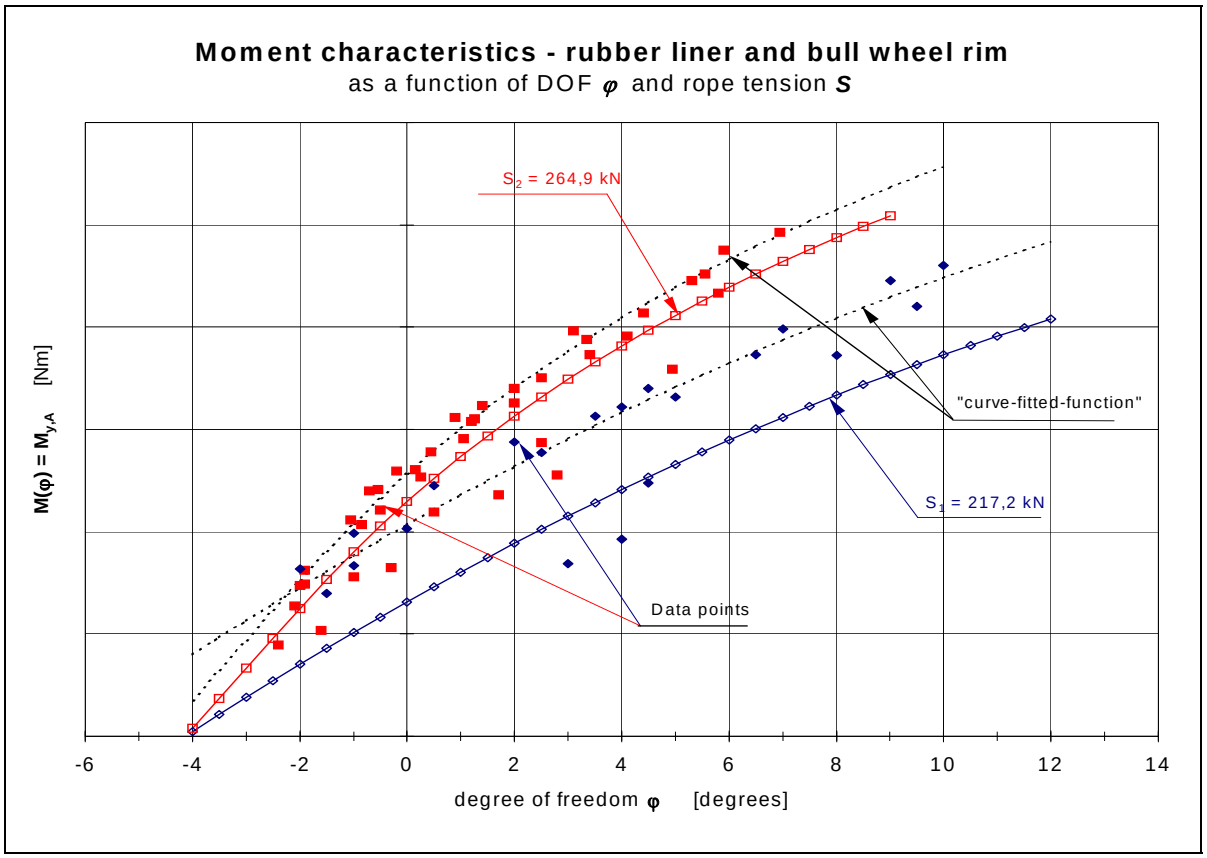

Fig. 6: Moment characteristics of the rubber liner

The Spring Characteristic of the Hold-Down Ring

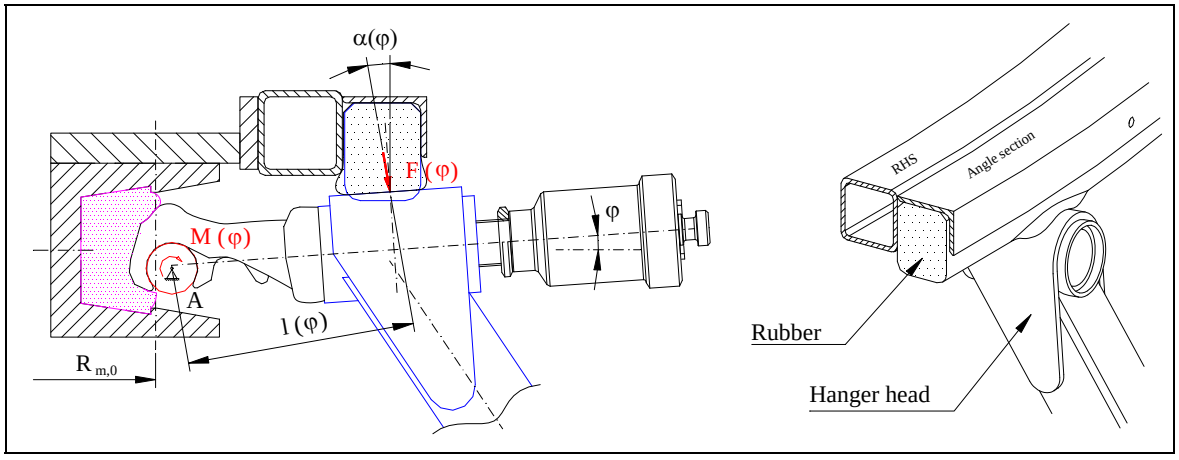

Fig. 7: Function schematic of the hold-down ring

The basic aim is to ensure that the vibration amplitudes of the chair to not become excessive as it follows its curved path. In order to satisfy this requirement an additional

hold-down ring has to be fitted to the top of the bull wheel (see Fig. 7). Although it prevents large amplitudes, at the same time it also causes increased stress in the hanger arm and in the chair itself.

The hold-down ring consists of an all-round steel construction (RHS + welded-on angle section) and a rubber insert. As the steel construction is very stiff (resistant to both bending and torsion), it is the rubber which largely determines the spring characteristic of the hold-down ring.

For the above reasons only the stiffness of the rubber is considered, thus dealing with the problem of the contact between the rubber and the hanger head.

The nonlinear contact problem (hyperelastic material behavior, large displacements/-strains as well as 3-D friction contact) is solved with the aid of an FE analysis. A 5-degree rubber segment is modeled, taking advantage of its symmetry. The hanger head is connected to a very stiff beam mounted at the theoretical point of rotation A so that the grip can be rotated incrementally (DOF φ) to impose a load.

Fig. 8 shows the deformed FE model and the distribution of the effective stress in the rubber when the grip is rotated through $\varphi = -7.4$ degrees.

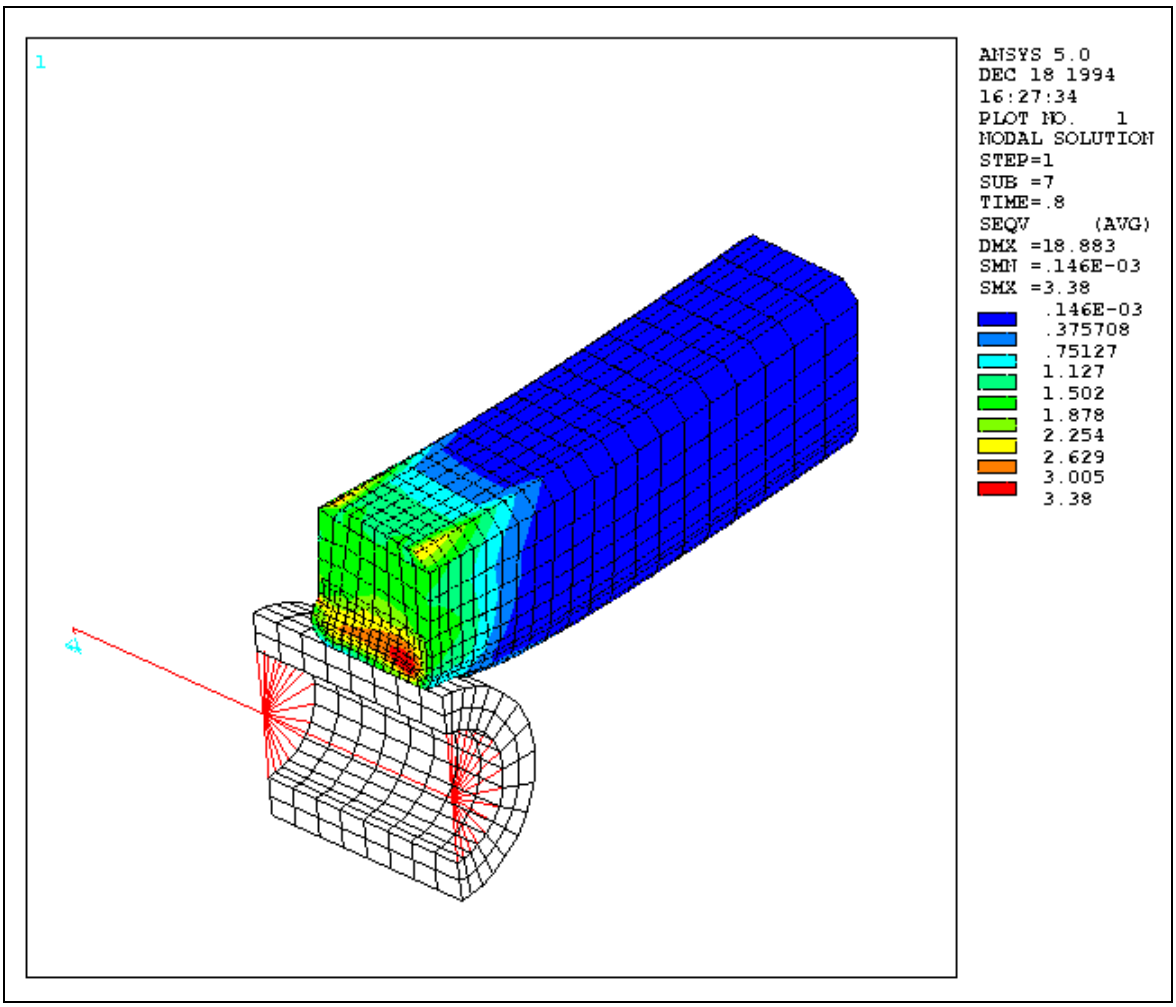

Fig. 8: Deformed FE model, von Mises stress in the rubber

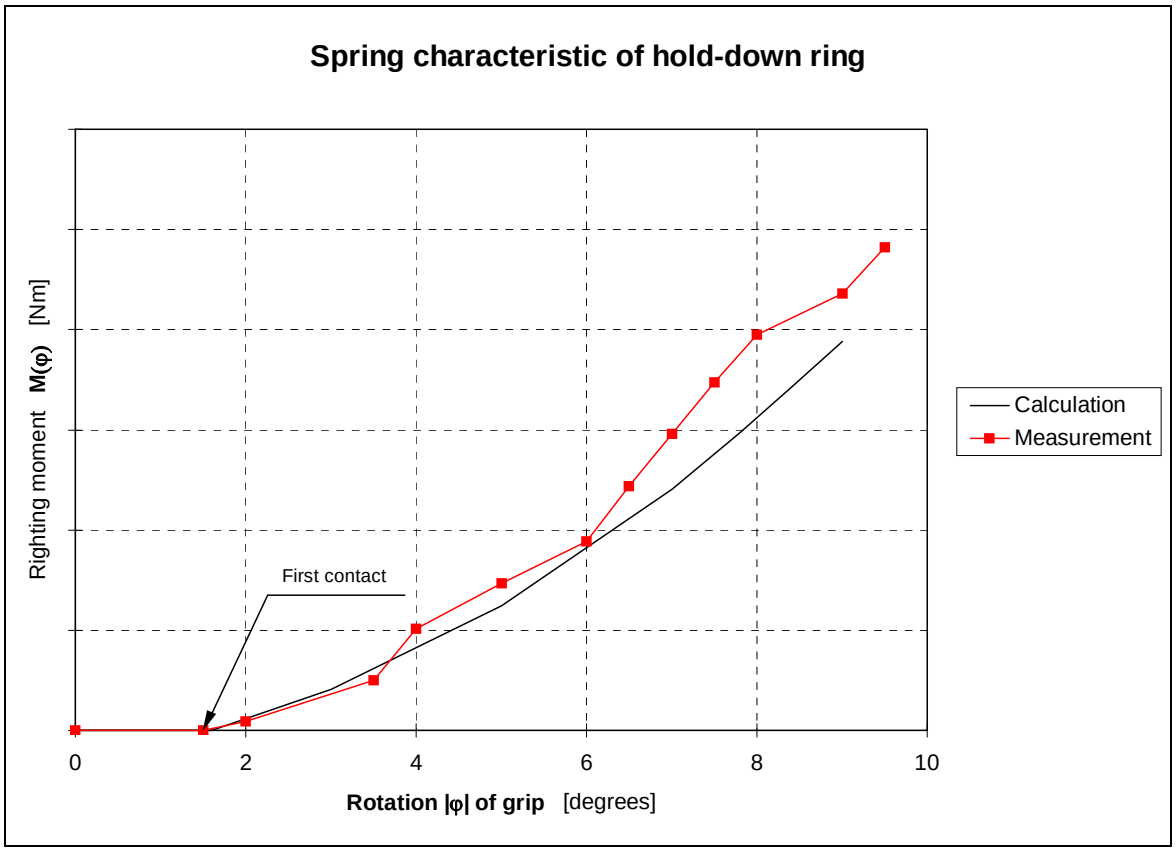

Fig. 9: Calculated hold-down ring characteristic

The Spring Characteristic of the Chair Guide Ring

The basic problem here is that of 3-dimensional, nonlinear stiffness. The nonlinearity results from the all-round rubber cushion which acts as a damping element between the ring and the hanger arm which strikes it. From a mechanical point of view, we are dealing with a series connection between two springs (see Fig. 10). This means that the resultant spring resistance is smaller than that of the complete steel ring alone including the 12 feet.

Since the complete ring construction does not only move in the direction of a force applied to it (see Fig. 10), $\boldsymbol{k}_1$ and $\boldsymbol{k}_2$ are matrices. These stiffness matrices represent a spring where the point at which force is applied can be moved at random in plane.

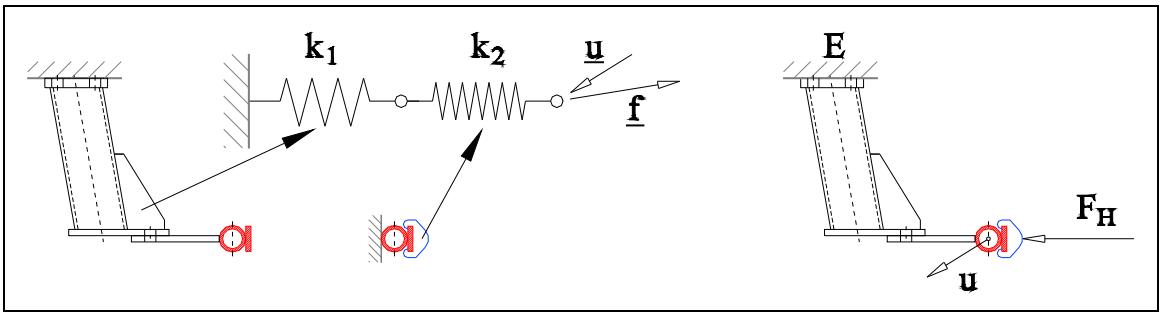

Fig. 10: Mechanical system for the guide ring

For the purposes of determining the spring characteristic – the stiffness of the ring depends on the position of hanger arm which, however, does not change as it passes around the bull wheel – the problem can be divided into two sub-problems:

- 3-dimensional, linear beam model

The beam model is used to determine the spring characteristic of the complete steel construction in relation to the position of the hanger arm. The object of this analysis is to calculate the stiffness matrix $\boldsymbol{k_1}$.

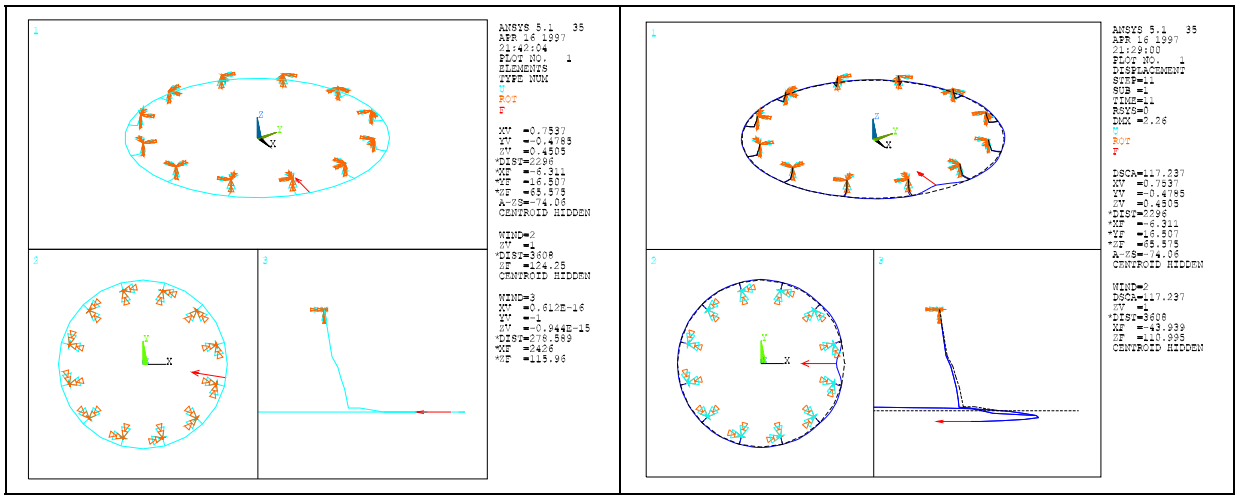

Fig. 11: Schematic of a 3-dimensional beam model.

The stiffness behavior of the steel construction is calculated with an FE program. The FE model used and a deformed structure under a horizontal load of 1 kN are shown in Fig. 11. It can be clearly recognized that the load point drops under a purely horizontal

load. The elements which do not disappear outside the main diagonal in the stiffness matrix $\boldsymbol{k}_1$ are characteristic of this coupling. Figure 12 shows a schematic of the individual matrix elements in relation to the load points over one half of a ring segment.

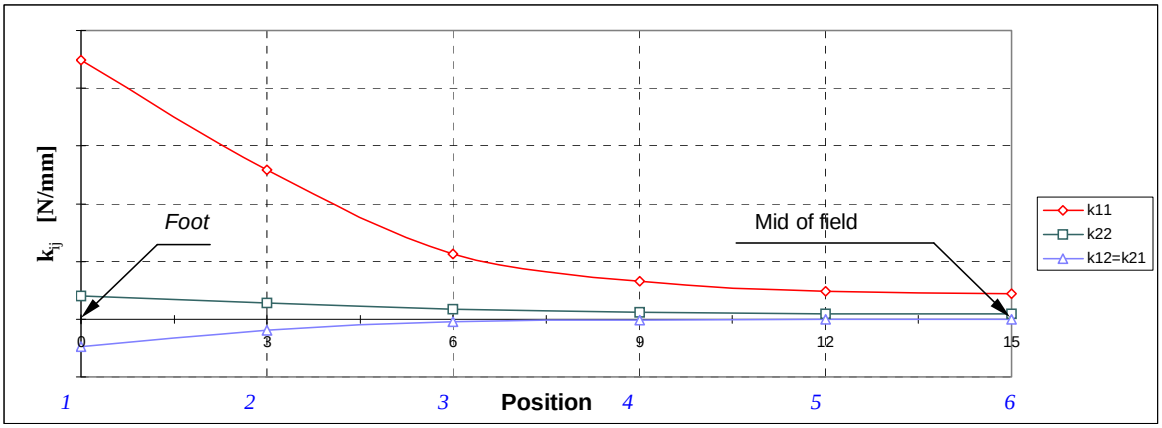

Fig. 12: Graphic representation of the individual matrix elements $\boldsymbol{k_{ij}}$.

- nonlinear, 2-dimensional FE model

The influence of the rubber cushioning is obtained from a nonlinear, rotationally symmetrical FE analysis. The nonlinearity of the analysis is not just limited to the hyper-elastic behavior of the rubber material. Large displacements/strains as well as contact with friction must also be taken into account.

Figure 13 shows a graphic representation of the spring force F_{res}, its horizontal and/or vertical component and the angle α (angle between spring force and the vertical) in relation to the depression into the rubber by the hanger arm.

The effective spring force acting on the hanger arm is derived from the series connection of the two springs.

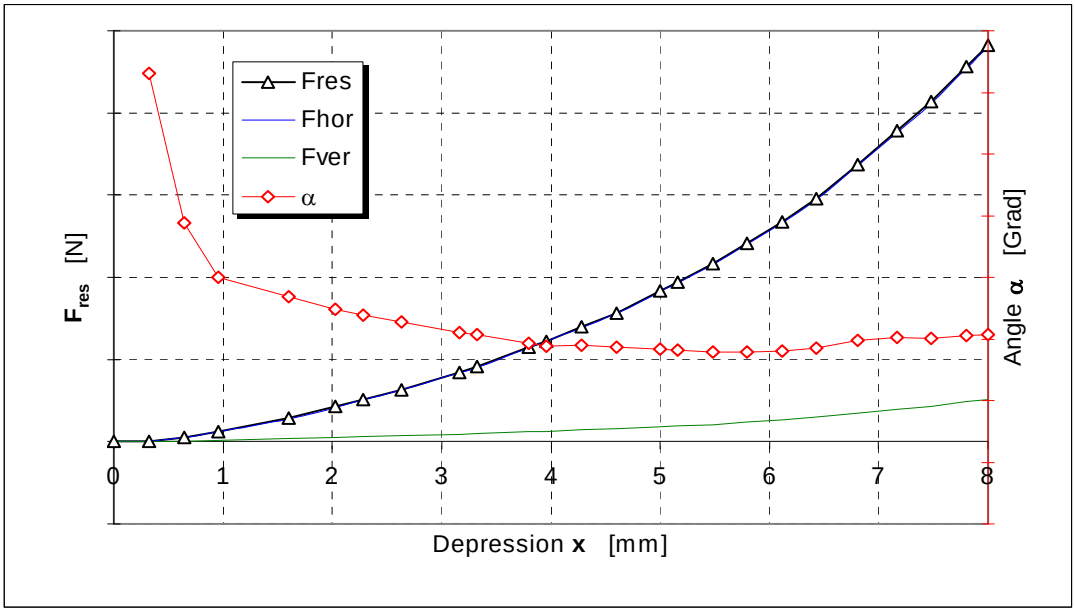

Fig. 13: Spring force F_{res} and angle in relation to depression of rubber by hanger arm

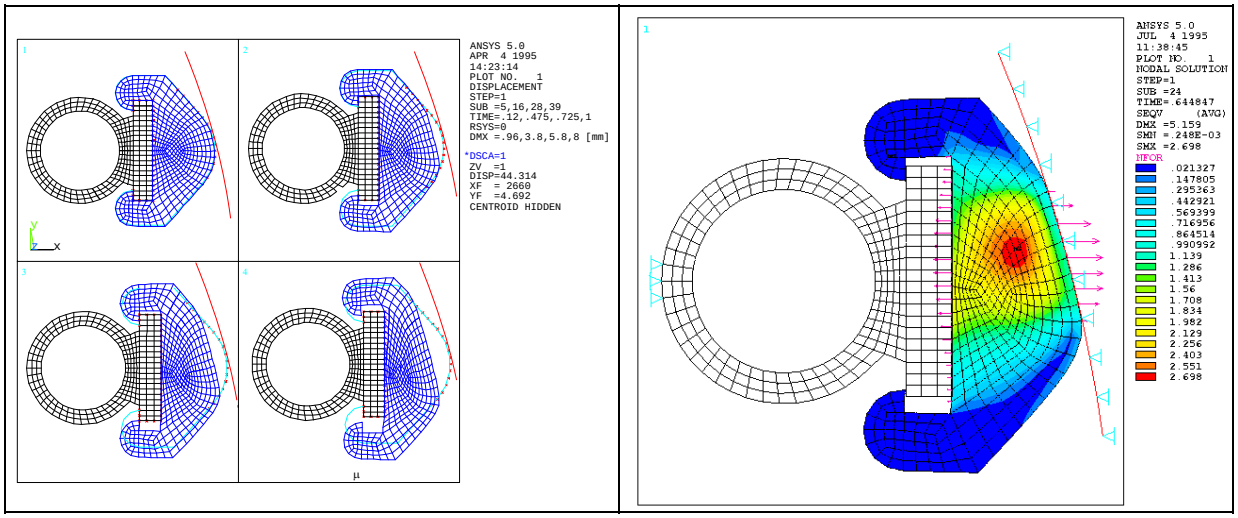

Fig. 14: Deformations of the FE model during various time increments of the calculation.

Masses and Moments of Inertia

For the purposes of the simulation, the masses and moments of inertia for the three different bodies – rope grip, hanger arm and chair – must be known as precisely as possible.

All components were therefore drawn in a CAD program as solids and the appropriate densities assigned to them (ρ = known mass/volume). The axial moments of inertia were then calculated by the program.

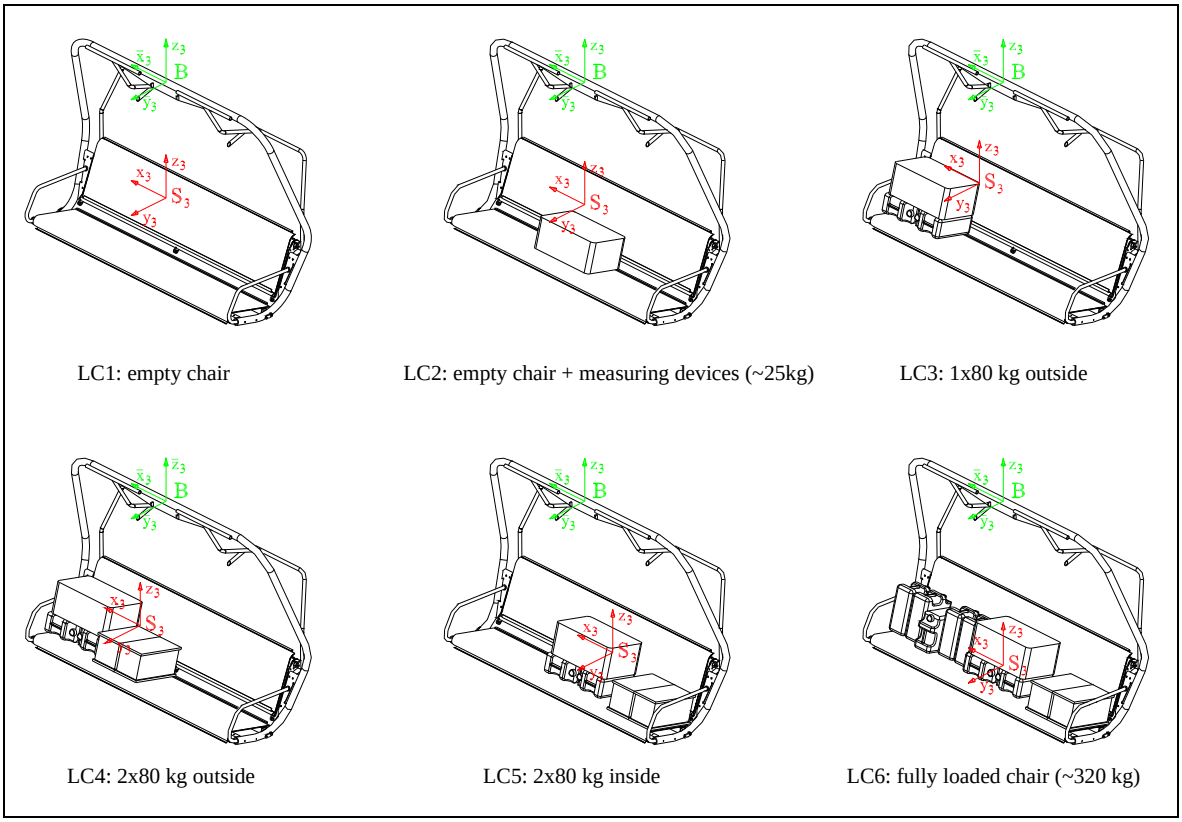

Fig. 15: Doppelmayr quad chair Model E / various load cases.

Equations of Motion

If, in addition to the movements of the chair as it passes around the bull wheel, we also consider points in time prior to and/or after bull wheel, then we have to distinguish between three phases in the simulation:

Phase 1: idealized straight path of travel prior to the chair entering the bull wheel,
Phase 2: passage around the bull wheel,
Phase 3: straight path of travel after leaving the bull wheel.

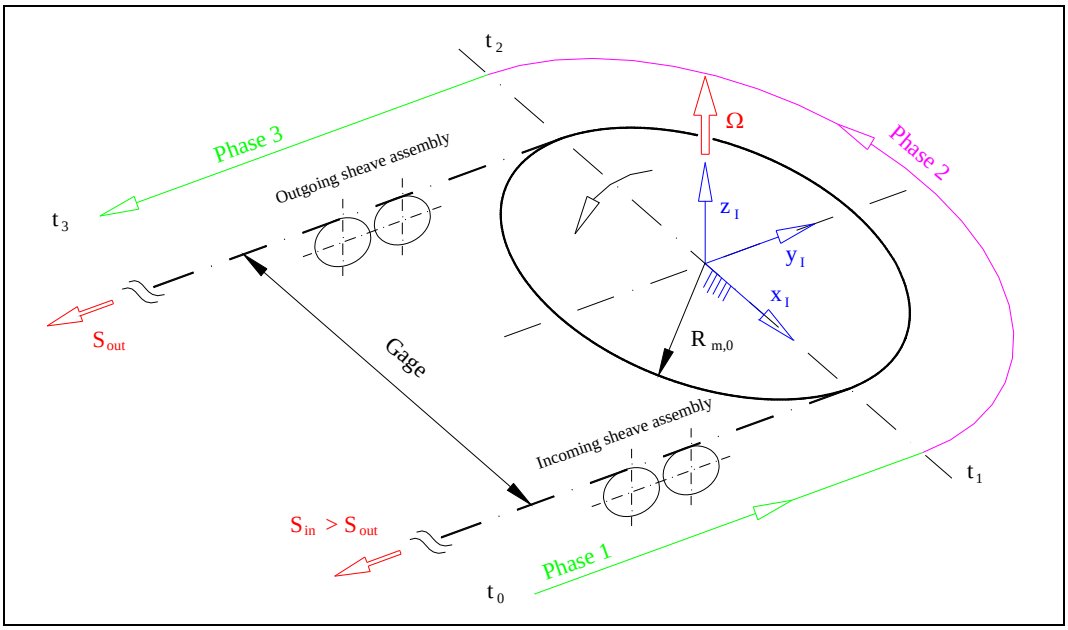

Fig. 16: The individual phases of the simulation.

From a mechanical point of view, the three simulation phases represent different system statuses, while the final status (velocities and acceleration rates of DOFs) of one phase simultaneously constitutes the initial status of the next phase.

In order to be able to calculate movements of the centers of gravity under known initial conditions, the equations of motion

$$m_i \underline{a}_{i/i} = \underline{F}_{i/i} \,, \qquad (3)$$

$$\mathbf{I}_{i/i}\,\underline{\alpha}_{i/i} + \underline{\tilde{\omega}}_{i/i}\,\mathbf{I}_{i/i}\,\underline{\omega}_{i/i} = \underline{M}_{i/i} \,. \qquad (4)$$

must be established for each individual body. However, $\underline{F}_{i/i}$ and $\underline{M}_{i/i}$ only represent ”external” forces acting on the bodies under consideration. Internal forces (e.g.: joint forces) are not included.

For the sake of brevity, a description of how the equations of motion are derived is not included.

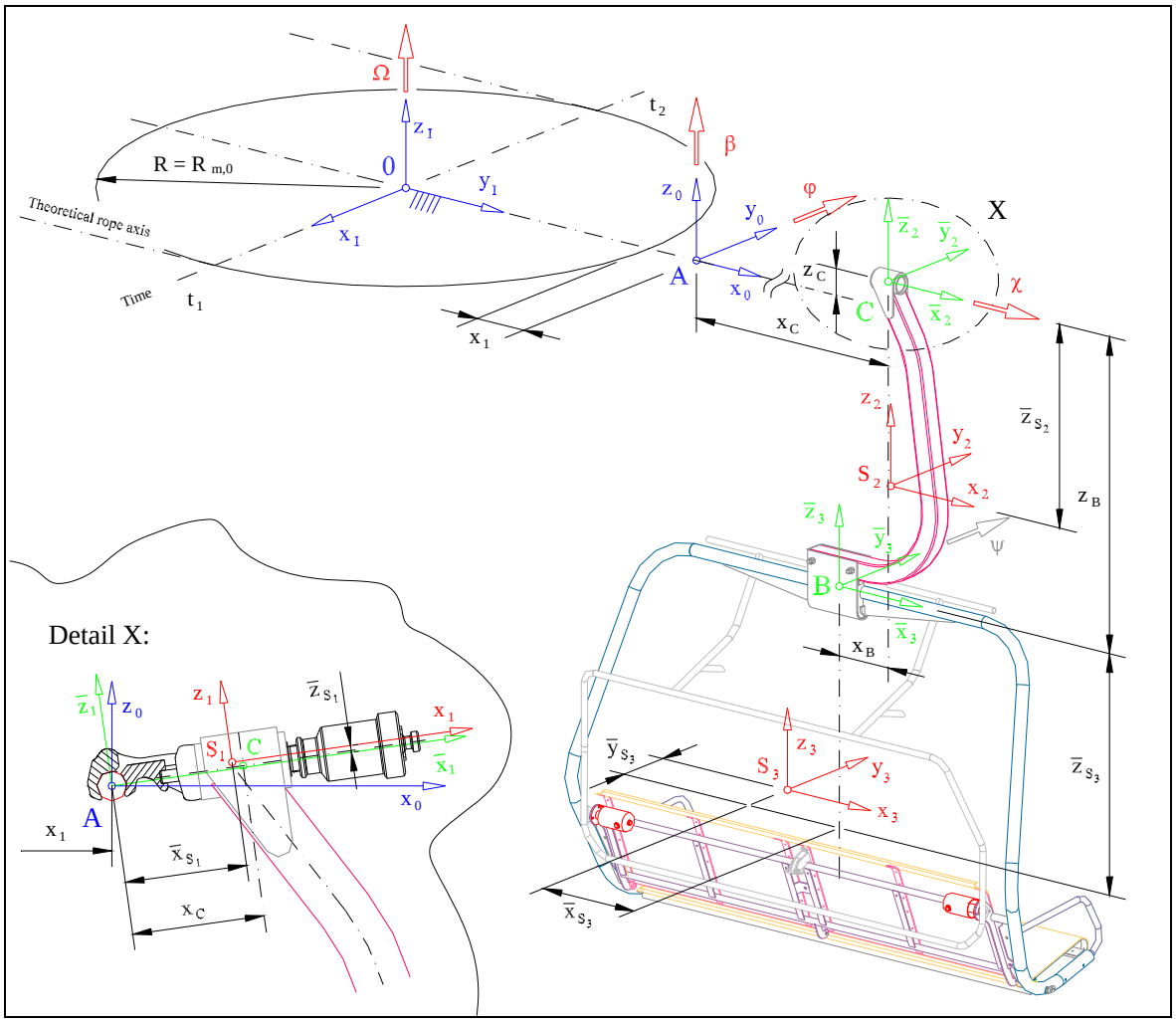

Fig. 17: Schematic of the geometrical configuration as the chair passes around the bull wheel

By integrating the equations (3) and (4) according to time, it is possible to calculate the complete sequence of movement.

Loads acting upon the Rope Grip

In order to be able to calculate the section forces at any cross section through the grip (e.g. section cut A-A, Fig. 18), the forces and moments transmitted in joint C as well as the reaction forces in point of rotation A must be known, in addition to the external forces and moments. The Newton/Euler equation must again be applied to the grip and

hanger arm, each of which is considered in isolation, so that these constrained forces can be determined.

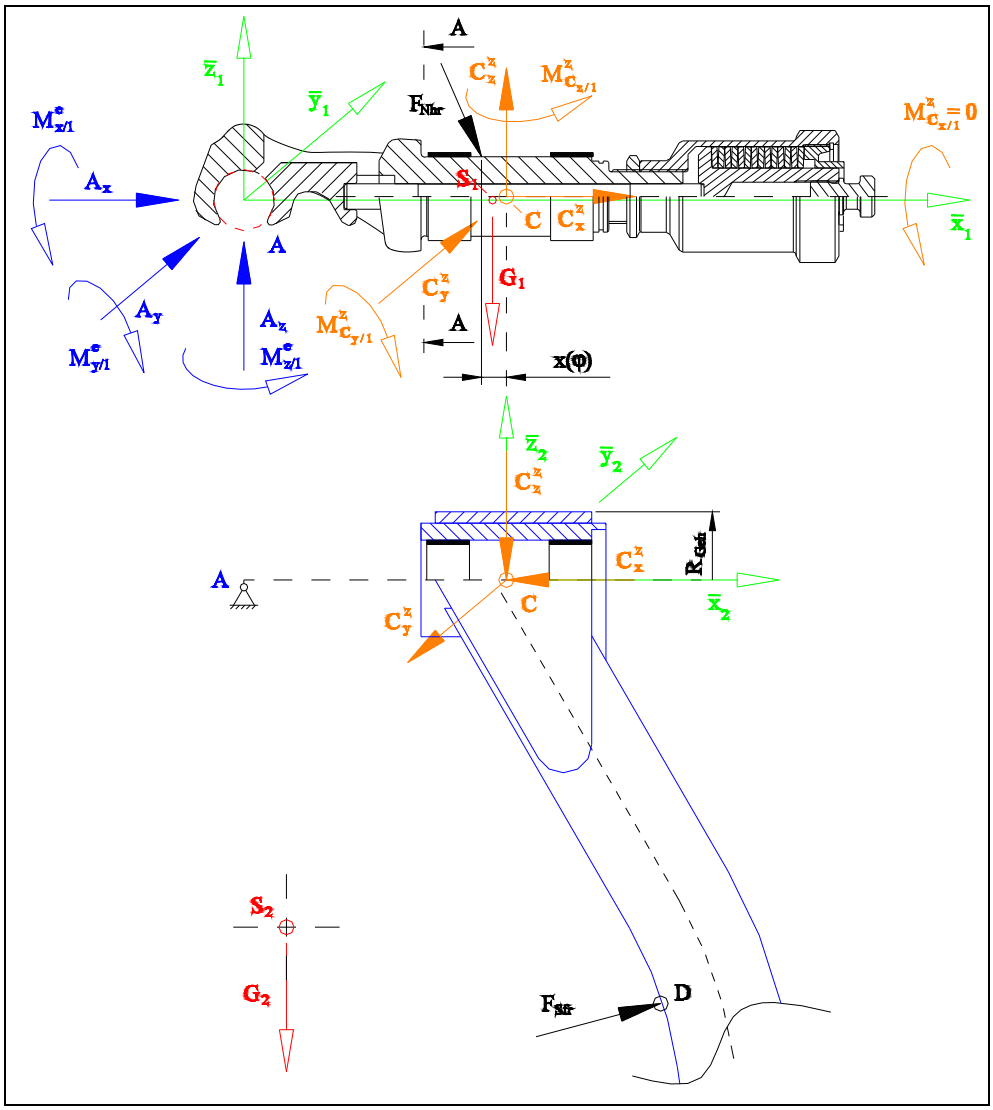

Fig. 18: Forces and moments acting upon the rope grip

The forces in joint C can be derived from the Newton equation calculated for the hanger arm (body 2):

$$\underline{C}_{2/2}^z = m_2 \mathbf{J}_{C_2/2} \ddot{\underline{z}} + m_2 \underline{a}_{2/2}^* - \underline{F}_{2/2}^e . \qquad (5)$$

The reaction forces in point A are then obtained from the Newton equation for the rope grip:

$$\underline{A}^{z}_{1/1} = m_1 \mathbf{J}_{C_1/1}\,\underline{\ddot{z}} + m_1\,\underline{a}^{*}_{1/1} - \underline{F}^{e}_{1/1} - \underline{C}^{z}_{1/1} \qquad (6)$$

The moments in joint C have to be determined with the aid of the Euler equation for the rope grip:

$$\mathbf{I}_{1/1}\mathbf{J}_{\omega 1/1}\,\underline{\ddot{z}} + \mathbf{I}_{1/1}\,\underline{\alpha}^{*}_{1/1} + \left(\mathbf{J}_{\omega 1/1}\,\underline{\dot{z}} + \underline{\tilde{\omega}}^{*}_{1/1}\right)\mathbf{I}_{1/1}\left(\mathbf{J}_{\omega 1/1}\underline{\dot{z}} + \underline{\omega}^{*}_{1/1}\right) = \underline{M}^{e}_{1/1} + \underline{\mathrm{M}}^{z}_{\mathrm{A}_{1/1}} + \underline{M}^{z}_{C_1/1}\,. \qquad (7)$$

Finally, it should be pointed out that joint C cannot transmit any moments about the $\bar{x}_2$ axis as body 2 has a DOF in this direction. A calculation performed to cross check the values taken from the simulation confirms that this is in fact the case, i.e. that the moment $M^{z}_{C_x}$ always results in zero.

Since all forces and moments are known, the section forces acting on the grip in any cross section can be calculated by reducing the spatial force system.

The Simulation Program SIMCHAIR

The simulation program is the very core of this paper. It was developed as a numerical solution of the nonlinear equations of motion and for calculating the joint forces. SIMCHAIR reads in the required input data (distances between joints, center of gravity coordinates, masses, etc.) from a formatted input file. After a successful run, the results required by the user are stored in different files.

The computer program was written on a Personal Computer (PC) in the object-oriented programming language C++. It is basically modular in structure, i.e. major functions, such as e.g. the integration algorithm, constitute independent parts of the program. Figure 19 shows a schematic of the individual modules and how they are interlinked. The arrows symbolize access to a module.

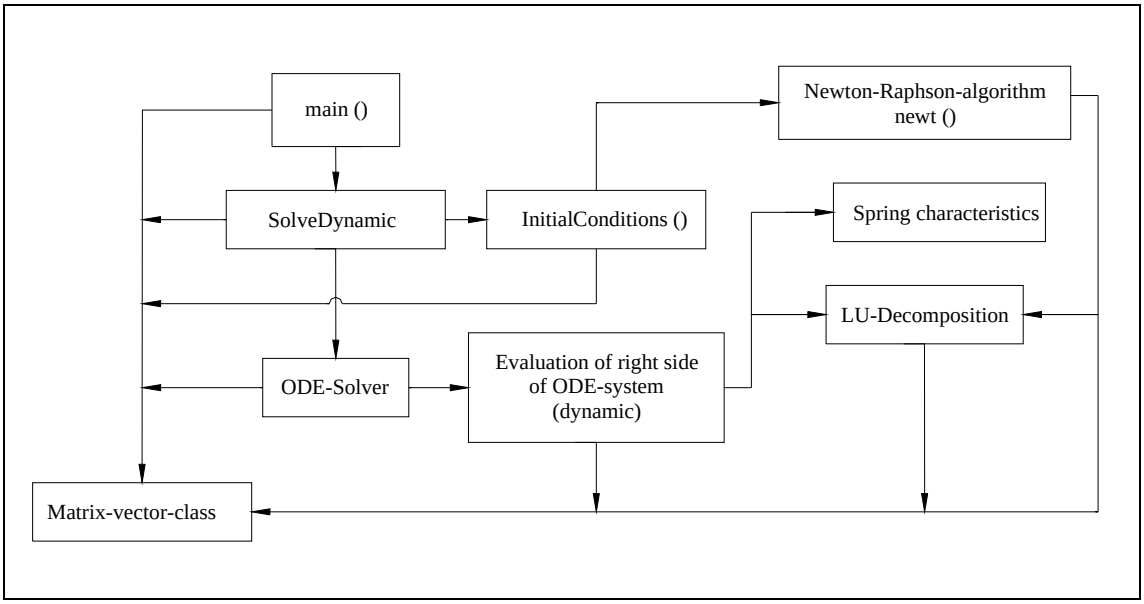

Fig. 19: Module hierarchy of the simulation program SIMCHAIR

Results of the Simulation Runs

In order to verify the rigid body program ”SIMCHAIR”, it was used to calculate several simulation runs. System statuses obtained during measurement were used for the loads acting on the dynamic model to allow direct comparison with the trial. These involve various load conditions of the carrier used for measurement purposes, and different rope speeds. The joint forces $\underline{\overline{C}}^{z}_{1/1}$ and the joint moments $\underline{\underline{M}}^{z}_{C_1/1}$ are calculated for each load status (except load case 1 = empty chair) in accordance with rope speed.

Table 1 lists the various load cases for the carrier (see also Fig. 15).

The simulation results of two load cases which have been calculated with the rigid body program SIMCHAIR are illustrated below in schematic form.

LC	Description of Load Case	Total Mass	Initial Side Swing φ_0

[1]	[1]	[kg]	[degrees]
1	empty chair	173.13	0.10
2	empty chair + measuring devices	198.13	-0.16
3	1 × 80 kg outside	258.13	5.83
4	2 × 80 kg outside	333.13	4,99
5	2 × 80 kg inside	333.13	-7.02
6	fully loaded chair	483.13	0.0

Table 1: Description of various load cases and list of initial side swing angles φ_0.

Load Case 6 (fully loaded chair)

This load case generates the greatest stress on the rope grip. For this reason, particular attention was paid to the simulation and evaluation.

A comparison of the progression and magnitude of the stress occurring in cross section A – A of the rope grip shows that the results of the simulation largely correspond to the results of the test. Decisive features of the measuring results, such as e.g. the increase in the righting moment $M_{C_y/1}$ with increasing dwell time of the chair on the bull wheel, are reproduced. Vibrations about the vertical axis of the chair show virtually the same behavior as established by the elongation measurements.

Figures 20 - 21 show schematics of the joint forces and moments for a fully loaded chair (total mass ≈ 483 kg).

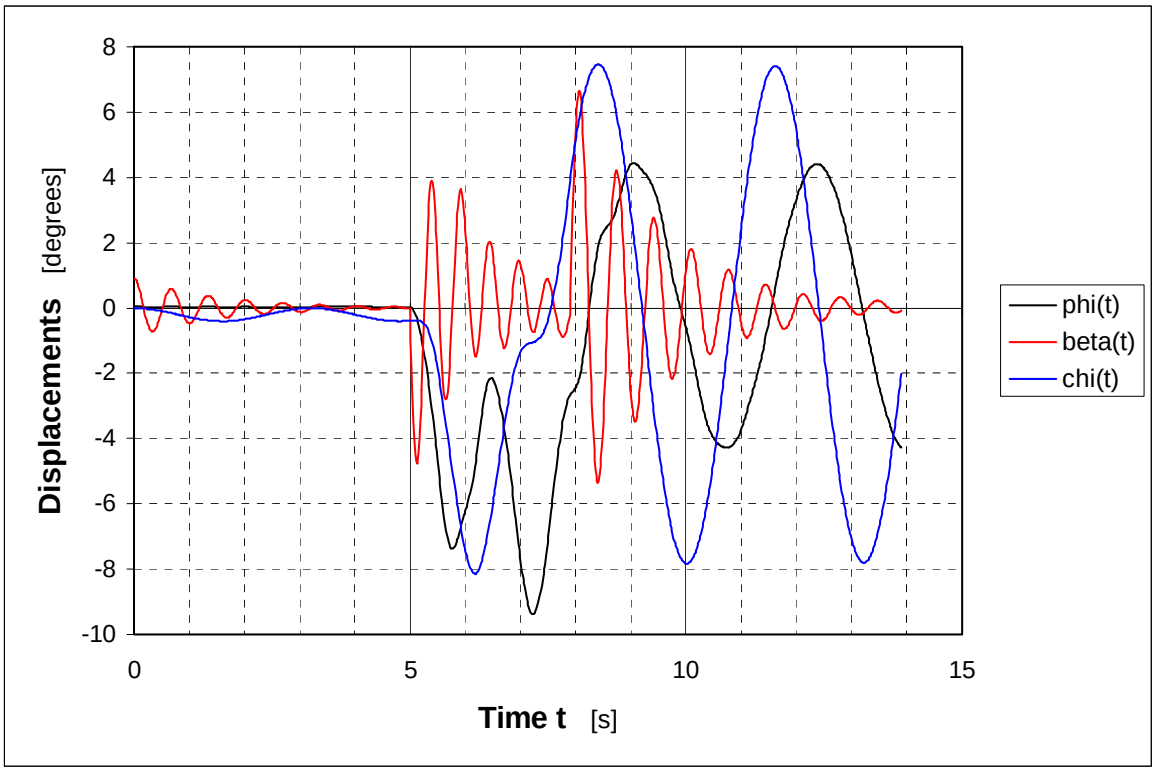

Fig.20: Displacements, Load Case 6 (LC6), rope speed v = 2.6 m/s.

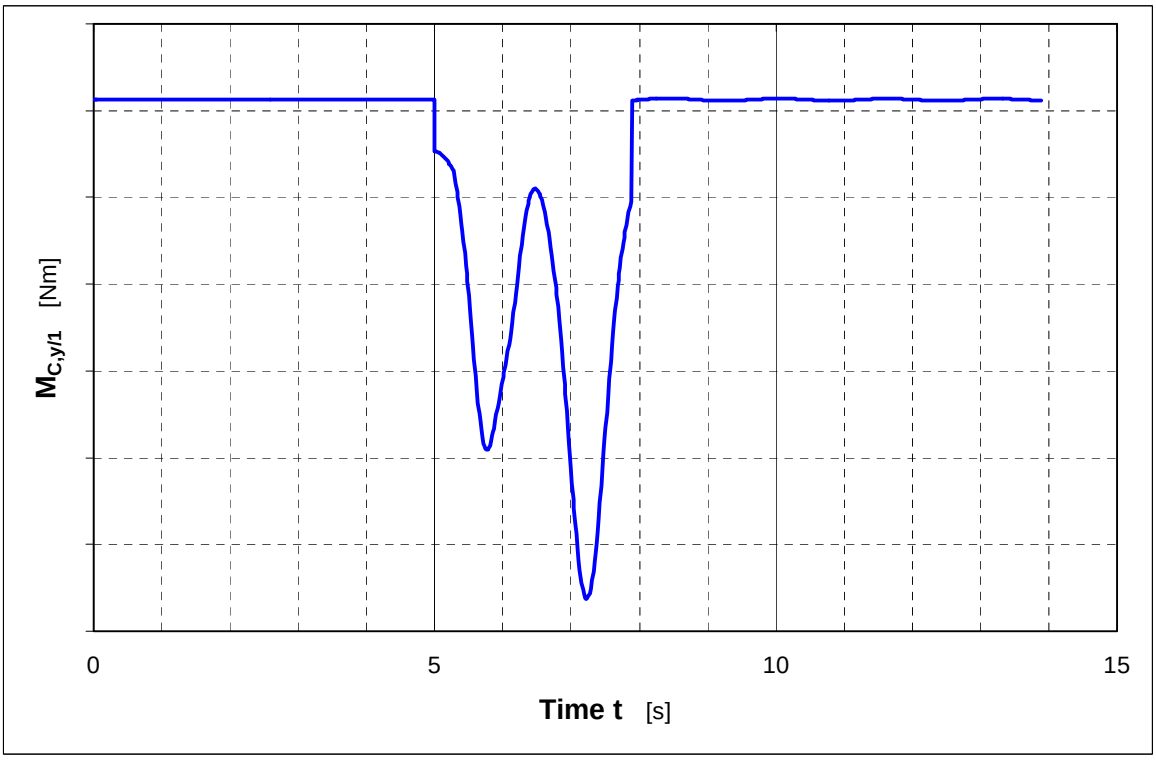

Fig. 21: Moment in joint C about the y axis, Load Case 6, rope speed v = 2.6 m/s.

Load Case 5 (inside of lift loaded with 2 × 80kg)

The greatest stress arises on entry into the bull wheel. As the geometrical configuration on entry into the bull wheel was not taken into account in the modeling of the hold-down ring, very large righting forces occur in the case of large initial displacements ($\varphi_0 \approx$ -7 degrees). However, these cause the large constrained forces in joint C. For this reason the maximum stress cannot be directly compared with the measurement results. If we consider the progression of section forces during the passage of the chair around the bull wheel, however, it is possible to establish a qualitative correspondence with the test results.

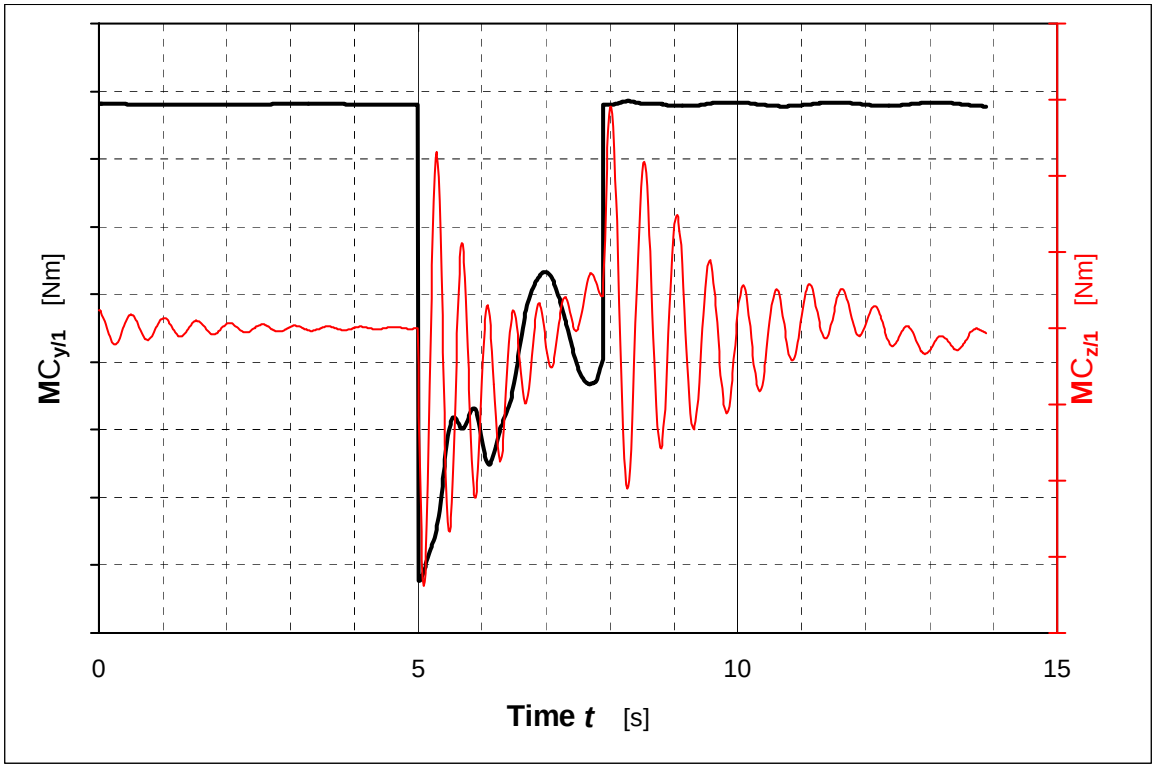

Fig. 22: Progression of moments in joint C for Load Case 5, rope speed of 2.6 m/s.

Summary

On fixed grip chair lifts, passage of the carriers around the bull wheel constitutes a critical type of stress. The main object of this paper was to develop a computer program which would make it possible to calculate the dynamic loads on the rope grip as it travels around the bull wheel. For the purpose of verifying the model and the computer program, a concrete chair lift on which stress measurements had been performed in June 1994 was recalculated.

After in-depth analysis of the mechanical problem, a rigid body model was developed. This model possesses three rotational DOFs and consists of two rigid bodies as well as several nonlinear springs and a damper. The spring characteristics were modeled as a substitute for various design measures and largely calculated using complex, nonlinear FE analysis. Available test results were also used to determine a moment characteristic.

For this rigid body model, equations of motion in accordance with Newton-Euler were established and implemented in a computer program. This program was developed on a PC using the object-oriented programming language C_{++}. It reads in an input file with a specific format, evaluates the parameters (e.g. joint coordinates, masses, center of gravity coordinates, moments of inertia, etc.) and finally resolves the dynamic problem of a carrier passing around the bull wheel with the aid of a numerical integration algorithm. System displacements and, if required, the acceleration rates and joint forces, are output into a file as the calculation results. With the aid of these joint forces it is possible to determine the section forces in any cross section of the rope grip.

In order to verify the simulation model developed, various movement sequences were simulated in several calculation runs. In each case, the chair loading corresponded to one test configuration, i.e. the geometrical and mechanical conditions were always comparable (same mass, etc.).

It was shown that the simulation model used contains all significant system parameters and provides useful qualitative and quantitative results for all relevant load cases.